Available online at www.sciencedirect.com
SCIENCE DIRECT®
Journal of Solid State Chemistry 176 (2003) 329–337
JOURNAL OF SOLID STATE CHEMISTRY
http://elsevier.com/locate/jssc

Sn/Sb atom ordering in the ternary stannide–antimonide TiSnSb

Enkhtsetseg Dashjav and Holger Kleinke*

Department of Chemistry, University of Waterloo, Waterloo, Ont., Canada N2L 3G1

Received 16 January 2003; received in revised form 7 April 2003; accepted 10 April 2003

Abstract

TiSnSb was prepared by reacting the elements Ti and Sb in an Sn flux at 500°C. Alternatively, TiSnSb can be synthesized from the elements in the stoichiometric 1:1:1 ratio at 850°C. According to our single crystal data, TiSnSb forms the Mg_2Cu type, orthorhombic space group *Fddd*, with $a = 5.4892(7)$, $b = 9.845(1)$, and $c = 19.151(3)$ Å ($Z = 16$). As evident from both our structure refinements and our electronic structure calculations, the two crystallographically independent positions of the Mg atoms in the Mg_2Cu type are not statistically occupied by the Sn and Sb atoms in the TiSnSb structure. Structural and electronic similarities to and differences from $TiSb_2$ and NbSnSb (both $CuAl_2$ type) are discussed. Supporting the electronic structure calculations, physical property measurements revealed the metallic character of TiSnSb, with holes being the dominant charge carriers.

Keywords: Crystal structure; Electronic structure; Physical properties; Titanium; Tin; Antimony

1. Introduction

The binary titanium stannides and antimonides form quite different compounds, with respect to both their formulas and their crystal structures. The binary Ti–Sn system contains four compounds (excluding high-pressure phases): Ti_3Sn [1], Ti_5Sn_3 [2], Ti_6Sn_5 [3] and Ti_2Sn_3 [4,5], while five antimonides have been published, namely Ti_3Sb [6], Ti_5Sb_3 [7], $Ti_{11}Sb_8$ [8,9], TiSb [10], and $TiSb_2$ [11]. Only the two most Ti-rich compounds have the same ratios of Ti to main group elements E (Ti_3E and Ti_5E_3), yet form different structures. Part of the Sb atoms in $Ti_{11}Sb_8$ may be replaced by Sn atoms in a disordered fashion [12]. To date, TiSnSb is the only ternary in the Ti–Sn–Sb system whose structure is not adopted by a binary Ti stannide or antimonide: TiSnSb was reported to crystallize in the Mg_2Cu type, as determined from X-ray powder data [13], whereas $TiSb_2$ occurs in the $CuAl_2$ type, and a "$TiSn_2$" is not known.

The question whether the Sb atoms show a clear preference for either of the two possible atomic positions of the Mg_2Cu type has yet to be answered. This is not a trivial problem, as Sn and Sb have very similar (yet not identical) scattering power both in X-ray and neutron diffraction experiments. Furthermore, the two different Mg positions of the Mg_2Cu type cannot be easily assigned to Sn and Sb just based on the different coordination spheres or on analogies to isovalent compounds. This procedure was chosen to postulate Sn/Sb ordering in the Zintl compound KSnSb, which is isovalent and isostructural with KSnAs [14,15]. In NbSnSb ($CuAl_2$ type) on the other hand, isovalent and isostructural with $TiSb_2$, only one position is present for the main group elements (unless the symmetry were reduced), which was assumed to be mixed occupied by Sn and Sb [16]. In the case of TiSnSb, we utilized sophisticated electronic structure calculations to investigate the site preferences in combination with an X-ray single crystal structure study. Both methods suggest the same ordering, thus confirming each other.

2. Experimental

2.1. Synthesis

TiSnSb was first prepared by a reaction of a 1:1 mixture of the elements Ti and Sb in an Sn flux. All three elements were used as obtained from ALFA AESAR in powder form, with metal-based purities between 99.5%

*Corresponding author. Fax: 519-746-0435.
E-mail address: kleinke@uwaterloo.ca (H. Kleinke).

0022-4596/03/$ - see front matter © 2003 Elsevier Inc. All rights reserved.
doi:10.1016/S0022-4596(03)00214-7

and 99.9%. The reaction mixture was heated in an evacuated silica tube placed in a resistance furnace at 500°C for a period of 7 days, and then slowly cooled down to 150°C within the next 7 days. Then, the furnace was switched off to allow for rapid cooling to room temperature.

After removing the Sn excess with moderately diluted HCl, pure TiSnSb in the form of microcrystalline powder with some well developed larger plate-like single crystals remained, as identified by X-ray powder diffraction using a position-sensitive detector (INEL, Cu$K\alpha_1$ radiation). This suggests that TiSnSb is the most Sn-rich compound in this system with a Ti:Sb ratio of 1:1 (under the reaction conditions applied). Rietveld refinements (fullprof) based on the Mg_2Cu type in the orthorhombic *Fddd* space group yielded lattice dimensions of $a = 5.4892(3)$, $b = 9.809(7)$, and $c = 19.142(7)$ Å.

To investigate the phase range of $TiSn_{1-\delta}Sb_{1+\delta}$, a set of reactions was carried out at 850°C, starting from the stoichiometric ratios of the target compounds {1 Ti: $(1-\delta)$ Sn: $(1+\delta)$ Sb}, with $\delta = 0.2$, 0.0, and −0.2. For only with $\delta = 0$ pure TiSnSb was obtained, we conclude that the phase range is very small, if not negligible.

Table 1
Crystallographic data of TiSnSb

Chemical formula, formula weight (g/mol)	TiSnSb, 288.34
T (K), λ (Å) of measurement	295, 0.71073
Crystal size (μm)	74 × 25 × 21
Space group, Z	*Fddd*, 16
a (Å)	5.4892(7)
b (Å)	9.845(1)
c (Å)	19.151(3)
V (Å^3)	1034.9(2)
μ (mm^{-1})	22.557
$F(000)$	1968
ρ_{calcd} (g/cm^3)	7.402
θ range for data collection	$4.3 < \theta < 33.1°$
Reflections collected	1194
Independent reflections (R_{int})	458 (3.37%)
Refinement method	Full-matrix least-squares on F^2
Data/restraints/parameters	458/0/17
Goodness-of-fit on F^2	1.09
$R(F_0)/R_w(F_0^2)$ with $I > 2\sigma(I)$ (all data)	2.65/6.10% (3.77/6.59%)
Extinction coefficient	0.0063(2)
Effective min. transmission	0.6063
Largest diffraction peak/hole (eÅ^{-3})	−2.65/1.47

2.2. Crystal structure determination

A plate-like single crystal was selected for the data collection on a Smart Apex CCD diffractometer (BRUKER) using Mo$K\alpha$ radiation. One set of 606 frames was collected with 0.3° scans in ω for exposure times of 60 s per frame at $\chi = 0$. The data were corrected for Lorentz and Polarization effects. An absorption correction was performed using the SADABS routine. The systematic absences suggested unambiguously the *Fddd* space group of the Mg_2Cu type. This type is comprised of three atomic positions, one of which (the Cu site in Mg_2Cu) is obviously filled by Ti atoms, which have the smallest scattering factor here. The other two positions (Wyckoff notations: 16*f* and 16*g*) may be occupied by either Sn and Sb atoms, or mixtures thereof. We refined two different models that both exhibit full ordering of the Sn and Sb atoms. In model I, the 16*f* site is filled by Sn atoms, and 16*g* by Sb, and model II shows the reverse occupancies, namely Sn on 16*g*, and Sb on 16*f*. According to the refinements using SHELXL [17], model I is preferred with $R(F_0) = 2.65\%$, compared to 2.72% for model II. The same trend is observed in the other residual factors [$R_w(F_0^2)$: 6.10% vs. 6.25%, goodness-of-fit: 1.09 vs. 1.10]. Therefore, model I was chosen as the more likely solution for Tables 1 and 2 and all figures in this work, while both models are compared in Tables 3 and 4.

2.3. Electronic structure calculations

We carried out self-consistent tight-binding *first principles* linear muffin tin orbitals (LMTO) calculations of both structure models, I and II, using the atomic spheres approximation (ASA) [18–20]. The calculation was done on the primitive cell, which contains four formula units of TiSnSb. In the LMTO approach, the density functional theory is used with the local density approximation (LDA). The integration in k space was performed by an improved tetrahedron method [21] on a grid of 621 independent k points of the first Brillouin zone. Void space was filled with two so-called empty spheres in the first Brillouin zone. As in the X-ray analysis, model I is preferred according to the electronic

Table 2
Atomic coordinates and anisotropic displacement parameters of TiSnSb[a]

Atom	site	x	y	z	U_{11} (Å^2)	U_{22} (Å^2)	U_{33} (Å^2)	U_{eq} (Å^2)
Ti	16*g*	1/8	1/8	0.99921(6)	0.0069(6)	0.0077(8)	0.0060(5)	0.0069(3)
Sn	16*f*	1/8	0.29520(6)	1/8	0.0097(3)	0.0113(4)	0.0058(2)	0.0089(2)
Sb	16*g*	1/8	1/8	0.54823(2)	0.0075(3)	0.0119(4)	0.0096(3)	0.0097(2)

[a] For Ti and Sb, $U_{23} = U_{13} = 0$, $U_{12} = -0.0012(6)$ and 0.0019(2) Å^2, respectively. For Sn, $U_{23} = U_{12} = 0$, $U_{13} = 0.0016(2)$ Å^2.

Table 3
Selected interatomic distances and –ICOHP values[a] of both models of TiSnSb (Mg_2Cu, I and II)[b]

	d (Å)	–ICOHP (I)	–ICOHP (II)
Ti–2Ti	2.818(1)	1.775	1.769
Ti–2E1	2.856(1)	1.686	1.722
Ti–2E1	2.934(1)	1.358	1.456
Ti–2E2	2.901(1)	1.585	1.456
Ti–2E2	2.961(1)	1.425	1.352
E1–2E1	3.162(1)	0.624	0.539
E1–1E1	3.351(1)	0.246	0.139
E2–1E2	2.941(1)	1.293	1.162
E2–2E2	3.367(1)	0.131	0.264

[a] –ICOHP values are given in eV per bond.
[b] Model I (the chosen one in Tables 1 and 2 and all figures): E1 = Sn, E2 = Sb; Model II: E1 = Sb, E2 = Sn.

Table 4
–ICOHP values[a] cumulated for one TiSnSb unit of both models I and II of TiSnSb and hypothetical TiSnSb in an ordered variant of $TiSb_2$ (*Fmmm*, III)

	–ICOHP (I)	–ICOHP (II)	–ICOHP (III)
Ti–Ti	3.550	3.538	3.354
Ti–Sn	6.088	5.616	5.568
Ti–Sb	6.020	6.356	6.028
Sn–Sn	1.494	1.690	1.306
Sb–Sb	1.555	1.217	1.372

[a] Cumulated –ICOHP values are given in eV per atom.

structure calculation, with a lower total energy of 16.4 kJ per mol TiSnSb.

The same method was employed to calculate the electronic structures of $TiSb_2$, hypothetical TiSnSb in the $TiSb_2$ structure, and elemental Ti and Sn for a detailed comparison of bond strengths.

2.4. Physical property determinations

Seebeck coefficients S were determined on a bar of the dimensions of $5 \times 1 \times 1$ mm, cold-pressed using a force of 10 kN. A commercial thermopower measurement apparatus (MMR Technologies) was used to determine S under dynamic vacuum in the temperature range 300–600 K, using a constant internal standard that determines the temperature difference. Silver paint (AMI DODUCO Technology) was used to create the electric contacts.

Specific resistivities ρ were measured using a four-point-method at the same bar that was used for the Seebeck coefficient determinations. A self-made device was used to determine the voltage drops ΔV over a distance of 2 mm at constant current of 30 mA under dynamic vacuum between 300 and 125 K, wherein cooling was achieved by helium compression.

3. Results and discussion

3.1. Crystal structure

Detailed descriptions of the Mg_2Cu type may be found in Ref. [16] that describes this type based on different atomic layers, comparing it to the Mg_2Ni and $CuAl_2$ types. Alternatively, one can describe the TiSnSb structure based on Ti-centered square antiprisms, whose corners are occupied by four Sn and four Sb atoms, with distances to the Ti center of 2.86 and 2.93 Å for the Sn atoms and 2.90 and 2.96 Å for the Sb atoms (Table 3). These are typical lengths for Ti–Sn and Ti–Sb bonds, as they also occur in the most Ti-poor binaries, namely between 2.85 and 3.09 Å in Ti_2Sn_3 and 2.84 Å in $TiSb_2$. All of these distances are slightly longer than the sums of Pauling's single bond radii of the elements involved ($r_{Ti} = 1.32$; $r_{Sn} = 1.42$, $r_{Sb} = 1.39$ Å) [22], and almost equivalent to the sums of Slater's covalent radii ($r_{Ti} = 1.40$; $r_{Sn} = 1.45$, $r_{Sb} = 1.45$ Å) [23]. That the Ti–Sn bonds are shorter than the Ti–Sb bonds is not surprising, despite the longer single bond radius of Sn, compared to Sb, as a slightly higher negative charge of Sb is expected based on the fact that Sb is the most electronegative element in TiSnSb.

The Ti-centered Sn_4Sb_4 antiprisms are interconnected via their square faces to form chains in TiSnSb (Fig. 1), a condensation that results in linear chains with Ti–Ti bonds of 2.82 Å, the shortest bond in the structure of TiSnSb.

The columns of antiprisms are connected via common edges to form layers. The TiSnSb unit cell comprises

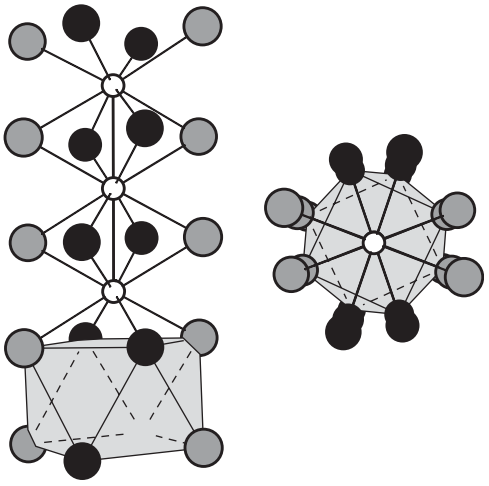

Fig. 1. The chain of Ti-centered Sn_4Sb_4 square antiprisms. Left: view from the side; right: from the top. White circles: Ti; black: Sn; gray: Sb atoms. Sn–Sn and Sb–Sb bonds are omitted for clarity.

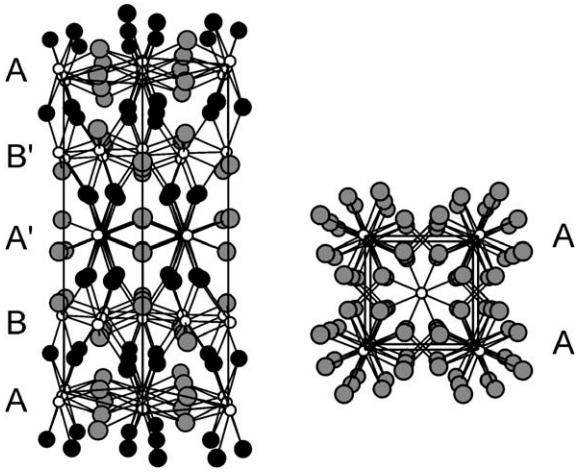

Fig. 2. Left: projection of the TiSnSb structure along [110]. Vertical: *c*-axis. White circles: Ti; black: Sn; gray: Sb atoms. Right: Projection of the $TiSb_2$ structure along [001]. Vertical: *a*-axis. White circles: Ti; gray: Sb atoms. Sn–Sn and Sb–Sb bonds are omitted for clarity.

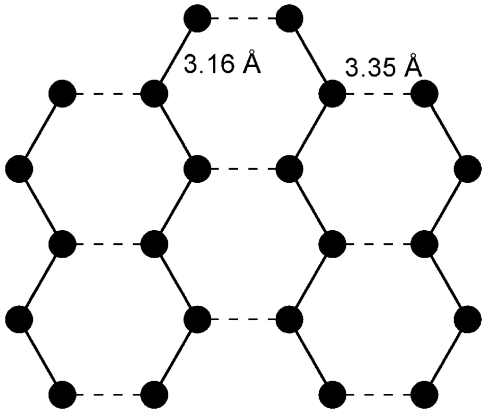

Fig. 3. The Sn atom substructure of TiSnSb. Horizontal: *b*-axis; vertical: *a*-axis.

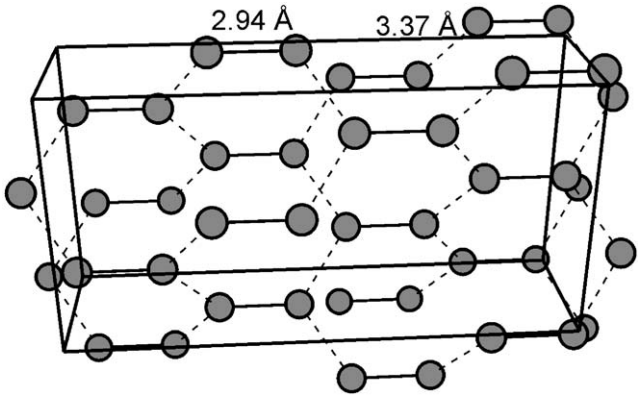

Fig. 4. Projection of the Sb atom substructure along the (slightly tilted) *a*-axis of TiSnSb. Vertical: *b*-axis.

four such (symmetry dependent) layers, which are stacked along the *c*-axis in the sequence ABA′B′. The Ti–Ti chains run parallel to [110] in A and A′, and parallel to $[1\bar{1}0]$ in B and B′ (left part of Fig. 2). A comparison with $TiSb_2$ ($CuAl_2$ type, also adopted by NbSnSb) is instructive: this structure exhibits topologically equivalent sheets of chains of antiprisms that are stacked in the simplest way along [100], namely eclipsed (AA, right part of Fig. 2).

Compared to TiSnSb, the Ti–Ti bonds in $TiSb_2$ (2.90 Å) are somewhat enlarged. Both distances, however, are indicative of strong Ti–Ti bonding, as a comparison with elemental titanium reveals, which is dimorph: in the hexagonal closed packing (Mg type), the interatomic distances are 6×2.89 and 6×2.95 Å, and in the body-centered cubic form (W type), the eight short bonds are 2.86 Å.

The arrangement of the Ti-centered Sn_4Sb_8 antiprism chains in TiSnSb leads to a clustering of the Sn atoms (denoted as E1 in Tables 3 and 4) in planar layers perpendicular to the *c*-axis. Such a layer, as depicted in Fig. 3, comprises Sn hexagons in a honeycomb-like setting. The hexagons are not regular, as each exhibits four shorter and two longer Sn–Sn bonds of 3.16 and 3.35 Å, respectively. Therefore, one may regard the Sn atom substructure as consisting of zigzag chains running parallel to the *a*-axis, that are interconnected via longer contacts to planar sheets comprising irregular hexagons. The Sn–Sn interactions of 3.16 and 3.35 Å may be compared to those in elemental (metallic) β-tin, which exhibits four Sn–Sn bonds of 3.02 and two of 3.18 Å. Similarly, the multitude of Sn–Sn distances in Ti_2Sn_3 ranges from 2.98 to 3.44 Å.

The Sb atom (denoted as E2 in Tables 3 and 4) substructure of TiSnSb is more complex than the Sn atom substructure, as it is extended three-dimensionally throughout the structure (Fig. 4). As with the Sn atom substructure, one can distinguish between a short and a long homonuclear bond, but with a much larger difference between the two contacts of 2.94 and 3.37 Å. This is reminiscent of elemental antimony, which comprises three short bonds of 2.91 Å and three longer bonds of 3.34 Å per atom. Such weakly yet definitely bonding Sb–Sb interactions of 3.2–3.4 Å are quite common in group 4 antimonides [9,24]. Ignoring the longer Sb–Sb contacts in TiSnSb in a first approximation, the Sb atom substructure consists solely of Sb atom pairs, which is also the case in the binary $TiSb_2$ with an Sb–Sb bond of 2.84 Å.

To summarize, there are significant differences between the Sn and Sb positions (E1 and E2) in the TiSnSb structure. First, the Ti–Sn bonds are shorter than the Ti–Sb bonds by an average of 0.04 Å. This can be understood based on the higher negative charge of Sb, compared to Sn, combined with equivalent covalent radii of the neutral atom (i.e. 1.45 Å). However, this is

not obvious to predict, as a neutral Sn atom comprises a shorter single bond radius than a neutral Sb atom.

Second, the homonuclear bonds differ both in their magnitudes and lengths. The Sn−Sn interactions resemble those of metallic β-tin, while the Sb−Sb interactions hint towards more localized bonding with the occurrence of one short bond and two much longer ones per Sb atom. So, while the differences are not that obvious, one might intuitively understand why the Sn and Sb atoms are ordered on the E1 and E2 sites in TiSnSb. More insight may be offered by a detailed analysis of the different bonding situations of the models I and II by utilizing the crystal orbital Hamilton population (COHP) tool [25], as discussed in the next section.

3.2. Electronic structure

Our electronic structure calculations revealed that the model I with the Sb atom on 16*g* (E2) is the preferred modification, based on a lower total energy of 16 kJ per mole TiSnSb compared to model II. Its band structure (symmetry lines chosen according to Bradley and Cracknell [26]) is depicted in the left part of Fig. 5, while the projection onto the densities of states (DOS) is shown on the right side.

The energy window chosen includes all filled valence bands, plus 2 eV above the Fermi level, E_F, which was arbitrarily placed at 0 eV. The differences in the electronegativities of the constituent elements (Sb > Sn > Ti) are reflected in the energetic order of the occupied bands. The lowest two bands (between −12 and −10 eV) have predominately Sb *s* character, followed by four overlapping bonds between −10 and −7 eV that are attributed pairwise to Sb *s* and Sn *s* orbitals. The other two Sn *s* bands are located around −6 eV. The block above −5 eV comprises mainly Sb *p*, Sn *p*, and Ti *d* dominated bands, with the latter starting to be filled at −2 eV. The small Ti contributions below −2 eV are indicative of covalent Ti−Sn and Ti−Sb bonding. No band gap is found in the vicinity of E_F, and the multitude of bands crossing the Fermi level along the lines $\Gamma - X$, $X - Y$, $Y - Z$ and $\Gamma - L$ point towards three-dimensional metallic properties of TiSnSb.

The existence of a local minimum in the DOS at approximately 0.5 eV above E_F suggests a transition from bonding to antibonding states. This can be verified by investigating the COHP that differentiate the states into bonding and antibonding contributions, the results thereof being comparable to the longer established crystal orbital overlap populations (COOP) [27] used to weigh the densities of states obtained via extended Hückel calculations [28,29].

All important COHP curves cumulated over the whole primitive cell (thus values given in [1/cell]) are shown in Fig. 6 in the same energy window as the band structure and the DOS. The Ti−Sn and Ti−Sb bonds seem to dominate the whole structure based on their multitude, while the Ti−Ti bonds stand out in a sharp bonding peak with its maximum slightly below E_F. Only bonding interactions are filled in all three cases, and the antibonding states would start to become filled about 0.5 eV above E_F, the above-mentioned local minimum in the DOS.

The situation is significantly different for both the Sn−Sn and Sb−Sb interactions (right part of Fig. 6). In both of these cases, some antibonding states are filled below E_F, while the bonding states clearly outweigh the antibonding ones by far. Both curves have similar shapes, in that the *s* states exhibit more bonding than antibonding states, which is also true for the *p* states. However, as the Sb−Sb curve is shifted towards lower energies by about 3 eV compared to the Sn−Sn curve, only the former has filled antibonding *p* states.

To provide more details on the different interactions of both of the structure models, the integrated COHP

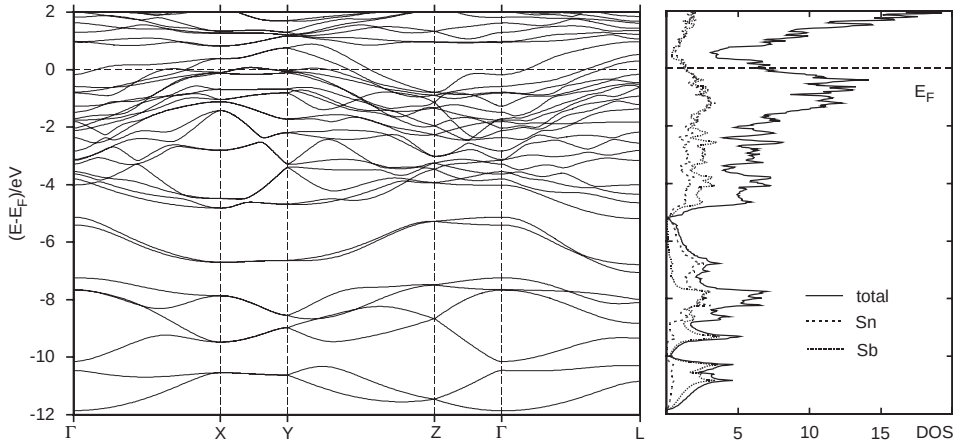

Fig. 5. Band structure (left) and densities of states (DOS, right) of TiSnSb.

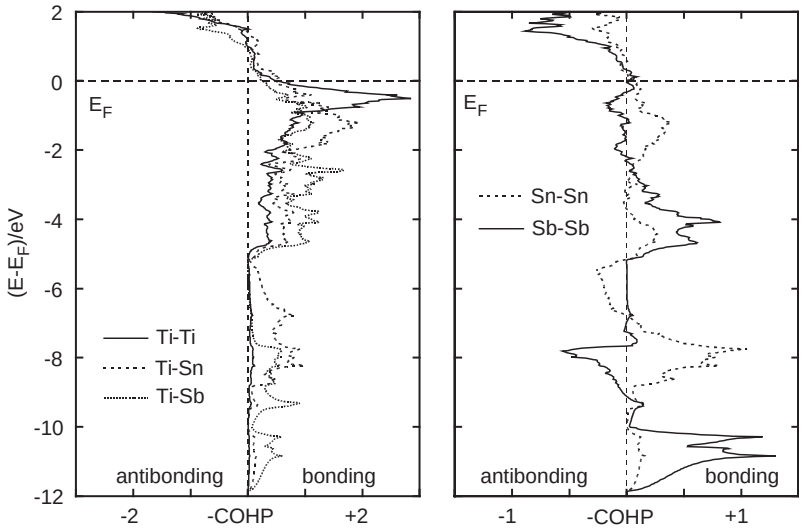

Fig. 6. Selected crystal orbital Hamilton population (COHP) curves of TiSnSb.

values (ICOHPs) of all interactions shorter than 3.4 Å is given in Table 3. The Sn–Sb distances between 3.54 and 3.68 Å all have negligible ICOHP values. When using the same energy scales, ICOHPs may be used to compare relative bond strengths in analogy to (but with higher accuracy than) the longer established Mulliken overlap populations (MOPs) [30] obtained from extended Hückel approximations. Strong bonds exhibit large positive MOPs, but large negative ICOHPs (or positive −ICOHPs), and ICOHPs have different units (eV instead of electrons per bond) and higher absolute values in the cases studied thus far. To our knowledge, the first published ICOHPs are −1.53 and −1.00 eV/bond for the shortest metal–metal bonds in elemental (bcc) iron and nickel, respectively [31].

All compounds and elements calculated by us for the comparisons had the Fermi level between −0.02 and −0.12 eV. In particular, both TiSnSb models were calculated to have the Fermi level at −0.08 eV. While this in itself is meaningless in LMTO calculations, the fact that comparable energies were used facilitates the ICOHP comparisons.

First, we compare the ICOHPs of the three kinds of homonuclear bonds of TiSnSb (model I, as this is the preferred modification) to the ICOHPs of the bonds in the corresponding elements, which we calculated for this purpose. The Ti–Ti bonds of the linear chain of antiprisms in TiSnSb (2.82 Å: −1.78 eV/bond) are shorter and stronger than the bonds in body-centered elemental titanium (2.86 Å: −1.46 eV), thus definitely strong bonding. The two Sn–Sn bonds of TiSnSb (3.16–3.35 Å: −0.62 to −0.25 eV) are very comparable with respect to both lengths (albeit roughly 0.2 Å longer) and strength to those of the elemental metallic form of tin (3.03–3.18 Å: −0.71 to −0.22 eV).

The short Sb–Sb bond of 2.94 Å of the Sb atom pair of TiSnSb is slightly longer than the shortest bond in the element (2.91 Å) and clearly weaker with −1.29 vs. −1.63 eV per bond. Similarly, the different Sb–Sb bonds of $MoSb_2S$ of comparable lengths (2.84–2.88) have an averaged ICOHP of −1.66 eV per bond [32]. On the other hand, the Sb–Sb bond of 2.91 Å in the Sb atom pair of Mo_3Sb_7 is much weaker with −0.79 [33], indicating that an often-postulated bond strength/length correlation is not obvious.

The longer Sb–Sb bond of 3.37 Å of TiSnSb compares better to the intermediate bond of the element (3.34 Å: −0.26 eV), with an ICOHP value of −0.13 eV, which is about 10% of the stronger bond.

Second, we turn our attention towards the heteronuclear interactions. The short Ti–Sn and Ti–Sb bonds (all between 2.86 and 2.96 Å) have ICOHP values between −1.36 and −1.69 eV per bond, i.e. values of the order of the Zr–Sb bonds in $Zr_{11}Sb_{18}$ [34]. For a better comparison, we calculated the ICOHP value of the Ti–Sb interaction of 2.92 Å of $TiSb_2$, which (with −1.52 eV) turned out to be within the range of the values of TiSnSb. It is concluded that all the selected interatomic distances given in Table 3 have bonding character, albeit of different strengths. Furthermore, a good correlation between bond strength and bond length is observed within the TiSnSb structure, but not necessarily in comparison to other compounds.

Third, the question remains in how far the two models I and II differ in their bonding situation. Model I, the one with the lower total energy and better refinement values, was determined in this work as the correct one. Therein, the Sb atoms are situated on a 16*g* site (E2), forming Sb–Sb pairs, whereas these pairs are formed by Sn atoms in model II. For a comparison of the two

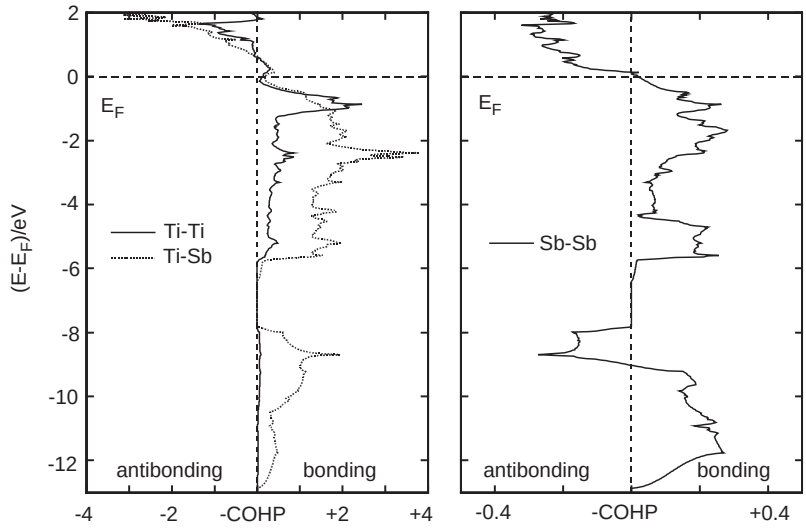

Fig. 7. Selected crystal orbital Hamilton population (COHP) curves of $TiSb_2$.

structure models, we listed the ICOHP values cumulated for each different bond kind per formula unit TiSnSb, i.e. Ti–Ti, Ti–Sn, Ti–Sb, Sn–Sn, and Sb–Sb, in Table 4. The Ti–Ti, Ti–Sn and Sb–Sb bonds per TiSnSb unit are stronger in model I by 0.01, 0.47, and 0.34 eV, respectively, while the Ti–Sb and Sn–Sn bonds are weaker by 0.34 and 0.20 eV, respectively.

Fourth, a comparison of TiSnSb (Mg_2Cu type) with $TiSb_2$ and NbSnSb (both $CuAl_2$ type) is instructive. Why is TiSnSb not isostructural with $TiSb_2$? Evidently the Sn atom is not the reason per se, for NbSnSb is isostructural with $TiSb_2$. More likely the overall valence-electron concentration per formula unit (TiSnSb: 13; $TiSb_2$ and NbSnSb both 14 electrons) is the driving force, as Ti and Nb are of similar (though not equivalent) size and electronegativity as are Sn and Sb. In theory, adding one valence electron to TiSnSb without changing the structure type would raise the Fermi level by almost 1 eV by filling two more bands per four TiSnSb units. As evident from the COHP curves shown in Fig. 6, this would not lead to overall significant increases in bond strengths, as more antibonding Sn–Sn and Sb–Sb states would become filled, while a gain in the Ti–Ti and Ti–Sn bonding would be achieved.

The COHP curves of $TiSb_2$ (Fig. 7) indicate that its 14 valence electrons may very well be used to maximize bonding (here: Ti–Ti, Ti–Sb, and Sb–Sb), in contrast to the hypothetical TiSnSb with 14 valence electrons. Only very few antibonding states well below E_F are filled in $TiSb_2$, namely the Sb–Sb antibonding *s* states at −8 eV. On the other hand, removing one electron from $TiSb_2$ (e.g. by replacing one Sb atom with one Sn atom) would decrease the strength of all interactions by depopulating bonding states, thus rendering this structure a less likely alternative for TiSnSb.

To verify this, we calculated the ICOHP values of hypothetical TiSnSb in the $TiSb_2$ structure, also summarized in Table 4. For that model, we chose an Sn/Sb ordering that minimizes the Sn–Sb contacts, as also found in the experimentally observed TiSnSb structure, resulting in a symmetry reduction from I4/*mcm* to *Fmmm*. Then, Sn–Sn as well as Sb–Sb pairs are present with interatomic distances of 2.84 Å, but no Sn–Sb distances shorter than 3.5 Å. It is evident that basically all cumulated −ICOHP values decreased from the model I to this hypothetical structure, namely for the Ti–Ti interactions from 3.55 to 3.35 (per Ti atom), the Ti–Sn interactions decreased from 6.09 to 5.57, Sn–Sn from 1.49 to 1.31, and Sb–Sb from 1.56 to 1.37 eV, while the cumulated Ti–Sb–ICOHP values remain almost unchanged (6.02 vs. 6.03 eV per Ti atom).

3.3. Physical properties

The band structure predicts metallic properties for TiSnSb. This was verified by physical property measurements (Fig. 8): the specific resistivity increases roughly linear with increasing temperature between 130 and 290 K. Its room temperature value of 0.55 mΩ cm is about 10 times higher than that of metallic tin and titanium (both: 0.04 mΩ cm), and 300 times higher than copper's resistivity at room temperature. That the TiSnSb resistivity is rather high for a metal suggests that a strong grain boundary effect is contributing to the measured value, which is not unexpected as the measurement was performed on a cold-pressed pellet. The Seebeck coefficients range from 8 to 14 μV/K between 300 and 600 K, indicating that holes are the dominant charge carriers. These values are typical for p-type metals, e.g. the group 4 metals zirconium

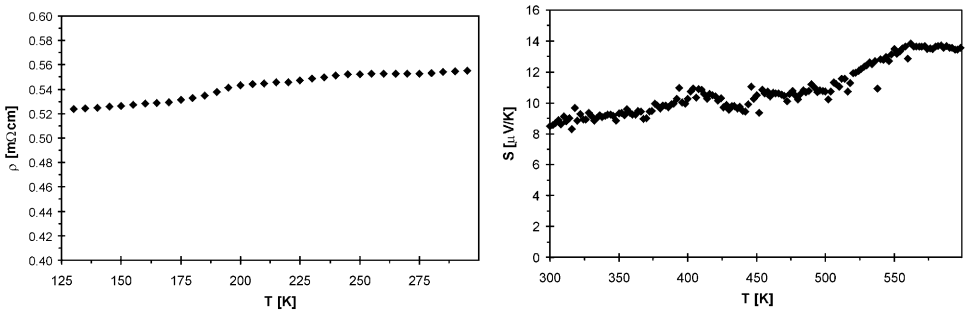

Fig. 8. Specific resistivity (left) and Seebeck coefficients (right) of TiSnSb.

(+8.9 μV/K) and hafnium (+5.5 μV/K at 300 K [35]) exhibit similar Seebeck coefficients.

4. Summary

The crystal structure of TiSnSb was determined via a combination of X-ray single crystal structure studies with LMTO calculations of the electronic structure. TiSnSb crystallizes in the Mg_2Cu type, while a "$TiSn_2$" is not known to exist, and $TiSb_2$ forms the $CuAl_2$ type. According to our investigations, the Sn and Sb atoms occupy well ordered the two different Mg sites of the Mg_2Cu type, with Sn on the 16*f* and Sb on the 16*g* site. This conclusion is supported both by experiment (i.e. better residual factors of the structure refinements—difference 2.6%) and as well as theory (i.e. lower total energy of this model, compared to the opposite ordering—difference 16 kJ per mole TiSnSb).

As a comparison of ICOHP values showed, this ordering maximizes in particular the Ti–Sn and Sb–Sb bonds, while the Ti–Sb and Sn–Sn bonds are weaker than in the hypothetical model with Sn on the 16*g* site. Sb atoms situated on 16*g* occurs with the formation of Sb–Sb pairs, as also observed in $TiSb_2$. Analogous Sn–Sn pairs are not present, and they are not found in the binary Ti/Sn system.

That TiSnSb is not isostructural to NbSnSb, which in turn is isostructural with $TiSb_2$, is a consequence of its smaller valence-electron concentration (13 instead of 14 electrons per formula unit). This became evident upon comparing the COHP curves of TiSnSb with $TiSb_2$.

As predicted via the band structure calculation and confirmed by two independent physical property measurements, TiSnSb is a metallic compound with small Seebeck coefficients.

Acknowledgments

Financial support from NSERC, CFI, OIT (Ontario Distinguished Researcher Award for H.K.), the Province of Ontario (Premier's Research Excellence Award for H.K.) and the Canada Research Chair program (CRC for H.K.) is appreciated.

References

[1] P. Pietrokowsky, Trans. Am. Inst. Min. 194 (1952) 211.
[2] P. Pietrokowsky, P. Duwez, Trans. Am. Inst. Min. 191 (1951) 772.
[3] K. Schubert, K. Frank, R. Gohle, A. Maldonado, H.G. Meissner, A. Raman, W. Rossteutscher, Naturwissenschaften 50 (1963) 41.
[4] H. Kleinke, M. Waldeck, P. Gütlich, Chem. Mater. 12 (2000) 2219.
[5] B. Künnen, W. Jeitschko, G. Kotzyba, B.D. Mosel, Z. Naturforsch. 55B (2000) 425.
[6] S. Ramakrishnan, G. Chandra, Phys. Lett. 100A (1984) 441.
[7] R. Berger, Acta Chem. Scand. 31A (1977) 889.
[8] H. Kleinke, Z. Kristallogr. Suppl. 16 (1999) 42.
[9] H. Kleinke, Chem. Soc. Rev. 29 (2000) 411.
[10] A. Kjekshus, F. Gronvold, J. Thorbjornsen, Acta Chem. Scand. 16 (1962) 1493.
[11] E.E. Havinga, H. Damsma, P. Hokkeling, J. Less-Common Met. 27 (1972) 169.
[12] H. Kim, M.M. Olmstead, J.Y. Chan, P.C. Canfield, I.R. Fisher, R.W. Henning, A.J. Schultz, S.M. Kauzlarich, J. Solid State Chem. 157 (2001) 225.
[13] B. Malaman, J. Steinmetz, J. Less-Common Met. 65 (1979) 285.
[14] K.-H. Lii, R.C. Haushalter, J. Solid State Chem. 67 (1987) 374.
[15] B. Eisenmann, J. Klein, Z. Anorg. Allg. Chem. 598/599 (1991) 93.
[16] T. Wölpl, W. Jeitschko, J. Alloys Compd. 210 (1994) 185.
[17] G.M. Sheldrick, SHELXTL-V5.1, University of Göttingen, Germany, 1998.
[18] O.K. Andersen, Phys. Rev. B 12 (1975) 3060.
[19] H.L. Skriver, The LMTO Method, Springer, Berlin, 1984.
[20] G. Krier, O. Jepsen, A. Burkhardt, O.K. Andersen, The TB-LMTO-ASA Program, Version 4.7c, MPI Stuttgart, Germany.
[21] P.E. Blöchl, O. Jepsen, O.K. Andersen, Phys. Rev. B 49 (1994) 16223.
[22] L. Pauling, The Nature of the Chemical Bond, 3rd Edition, Cornell University Press, Ithaca, NY, 1948.
[23] J.C. Slater, J. Phys. Chem. 41 (1964) 3199.
[24] H. Kleinke, J. Am. Chem. Soc. 122 (2000) 853.
[25] R. Dronskowski, P. Blöchl, J. Phys. Chem. 97 (1993) 8617; see also http://www.cohp.de.
[26] C.J. Bradley, A.P. Cracknell, The Mathematical Theory of Symmetry in Solids, Clarendon Press, Oxford, 1972.
[27] T. Hughbanks, R. Hoffmann, J. Am. Chem. Soc. 105 (1983) 3528.
[28] R. Hoffmann, J. Chem. Phys. 39 (1963) 1397.

[29] M.-H. Whangbo, R. Hoffmann, J. Am. Chem. Soc. 100 (1978) 6093.
[30] R.S. Mulliken, J. Chem. Phys. 23 (1955) 2343.
[31] G.A. Landrum, R. Dronskowski, Angew. Chem. Int. Ed. 39 (2000) 1560.
[32] C.-S. Lee, H. Kleinke, Eur. J. Inorg. Chem. (2002) 591.
[33] E. Dashjav, A. Szczepenowska, H. Kleinke, J. Mater. Chem. 12 (2002) 345.
[34] I. Elder, C.-S. Lee, H. Kleinke, Inorg. Chem. 41 (2002) 538.
[35] M.V. Vedernikow, V.G. Dvunitkin, A. Zhumagulov, Fiz. Tverd. Tela 20 (1978) 3302.